Contents lists available at ScienceDirect

Arabian Journal of Chemistry

journal homepage: www.ksu.edu.sa

Original article

Investigation of physico-mechanical, thermal, morphological, and antibacterial effects of bio-based epoxidized soybean oil plasticizer on PLA-ZnO nanocomposites as flexible food packaging

Mina Ghoroghi [a,1], Sara Estaji [b,c,1], Mohammad Iman Tayouri [a,b], Reza Jahanmardi [a], Marcos A.L. Nobre [d], Hossein Ali Khonakdar [b,*]

[a] Department of Polymer Engineering, Science and Research Branch, Islamic Azad University, Tehran, Iran
[b] Department of Polymer Processing, Iran Polymer and Petrochemical Institute, Tehran, Iran
[c] Department of Chemical Engineering, University of Tehran, Tehran, Iran
[d] São Paulo State University (Unesp), School of Technology and Sciences, Presidente Prudente, SP 19060-900, Brazil

ARTICLE INFO

Keywords:
Polylactic acid
Zinc oxide
Epoxidized soybean oil
Food packaging
Ductility

ABSTRACT

Polylactic acid (PLA) has attracted considerable attention because of its excellent properties compared to petroleum-based materials. However, improving its toughness, crystallization, and functionalities is challenging. Using a laboratory internal batch mixer, we produced unique blended nanocomposites comprising polylactic acid (PLA) as the host matrix, epoxidized soybean oil (ESO) as the plasticizer, and zinc oxide nanoparticles (ZnO NPs) as the reinforcements. The SEM-EDS test showed that neat PLA had a smooth surface, but the PLA-ZnO nanocomposite had rough micrographs and a uniform dispersion state of the nanoparticles. It was also found that adding ESO to the blend nanocomposites created a matrix droplet structure, and the size of the oil domains decreased as the ZnO content increased. All results derived from FTIR, XRD, and DSC tests were consistent with the morphological features in which ZnO NPs acted as the blend's compatibilizer and heterogeneous nucleating agent. Our team observed that adding ESO decreased the PLA-ZnO nanocomposites' glass transition temperature (T_g) by an average of 2 °C and increased the crystallization rate. It was also confirmed that the presence of ESO improved the flexibility and reduced the strength of the PLA. The tensile strength was further enhanced by incorporating ZnO into the blend. Adding 5 wt% of ZnO NPs increased the tensile strength of the PLA containing 10 wt% ESO by approximately 3.5 MPa. Furthermore, the tensile modulus was predicted using theoretical models; for example, the Paul model fitted with experimental findings. The addition of ESO increased the overall surface free energy of the nanocomposites. On the other hand, increasing ZnO content resulted in high contact angles and antibacterial properties of the blended nanocomposites. The favorable characteristics of the resulting films emphasized the potential use of these nanocomposite films as a promising choice for food packaging materials.

1. Introduction

Concerns regarding sustainable energy and environmental protection have prompted substantial studies on bio-resourced polyesters (Thakur et al., 2022). Therefore, the packaging industry is enthusiastic about creating biodegradable materials (Çoban et al., 2018; Khonakdar et al., 2024). Among the bio-polyesters on the market, polylactic acid (PLA) stands out for its several desirable properties, including its high processability and mechanical strength (Nofar et al., 2019; Mokhtari Aghdami et al., 2022; Anžlovar et al., 2018). However, PLA's price tag, intrinsic brittleness, lack of antibacterial activity, and slow crystallization rate limit its industrial packaging use (Murariu and Dubois, 2016). To tackle this issue, plasticizer addition, polymer mixing, coupling agents, co-polymerization, and nanotechnology are the keys to making eco-friendly composite materials with exceptional qualities (Mulla et al., 2021; Chausali et al., 2023; Ghassemi et al., 2022).

Over the past decade, the flexibility of PLA has improved using biodegradable plasticizers such as epoxidized soybean oil (ESO) (Jia

* Corresponding author.
E-mail address: h.khonakdar@ippi.ac.ir (H.A. Khonakdar).
[1] The contribution of the first and second authors is equal.

https://doi.org/10.1016/j.arabjc.2024.105928
Received 20 April 2024; Accepted 22 July 2024
Available online 25 July 2024

et al., 2018; Dare et al., 2024). The ESO can enhance PLA's cold crystallization performance and lower its glass transition temperature (T_g) (Xiong et al., 2013). This epoxidized vegetable oil can be synthesized from soybean oil molecules by epoxidation of C=C on their aliphatic long-chain portion. It should be highlighted that the epoxy functional groups presented on ESO chains are highly reactive with other moieties consisting of OH and COOH parts (Xu and Qu, 2009). Han et al. (Han et al., 2020) showed that ESO, at a low concentration (about 5 wt%), increased the elongation at break and tensile strength of the PLA-poly (butylene adipate-*co*-terephthalate) (PBAT) blend by 170% and 9 MPa, respectively. They stated that the ESO had effectively improved the compatibility of the PLA-PBAT blends. In another study, Raghunath et al. (Raghunath et al., 2018) pointed out that the ductility value of the PLA nanocomposites was improved by 108% when 20 wt% of ESO was added to the system. Furthermore, the addition of ESO to the PLA matrix significantly decreased T_g and cold crystallization temperature (T_{cc}), improving the crystallization process of the materials. Their research has shown that ESO's plasticizing impact notably increases the flexibility of PLA while reducing its strength and modulus. On the other hand, adding multi-walled carbon nanotubes (MWCNTs) to the blend could compensate for the reduction in modulus and tensile strength.

A new family of materials called polymeric blend nanocomposites reinforced with inorganic nanoparticles like zinc oxide (ZnO NPs) and titanium oxide (TiO_2) outperforms their unreinforced counterparts (Kango et al., 2013; Nazir et al., 2021). Among metal oxides, ZnO is prominent for its beneficial UV interactions with bacteria, considerable surface-to-volume ratio, improved mechanical characteristics, excellent optical absorption, and good thermal conductivity (Mallakpour and Behranvand, 2016; Tayebi et al., 2021). Additionally, ZnO NPs are currently recognized and classified as a safe substance (GRAS) by the Food and Drug Administration (FDA) (Espitia et al., 2012). Many studies have shown that metal oxides can kill bacteria through reactive oxygen species (ROS) production. For example, Tajdari et al. (Tajdari et al., 2020) reported that the ZnO enhanced the antibacterial activity of the PLA. It is also suggested that ZnO NPs act as heterogeneous nucleating agents to enhance the crystallinity of PLA and its strength (Yan et al., 2023). The enhanced mechanical properties and crystallization rate for PLA-ZnO nanocomposites, in which the improved T_{cc} resulted at lower temperatures, have been verified by Tang et al. (Tang et al., 2020). Their studies revealed excellent tensile strength but low flexibility in the PLA nanocomposites. Shojaeiarani et al. (Shojaeiarani et al., 2019) found that PLA-ZnO has a lower T_g than neat PLA, indicating that ZnO has a detrimental effect on PLA's molecular chains. Indeed, ZnO nanoparticles acted as catalysts against temperature. As a result, adding ZnO enhanced the crystallization rate of PLA. In distinct research, Kazemi-Pasarvi et al. (Kazemi-Pasarvi et al., 2020) fabricated PLA-polycaprolactone (PCL)-thermoplastic starch ternary blends incorporated with thymol and ZnO NPs. They investigated the contradictory effects of thymol as a plasticizer and ZnO as reinforcement on the chain increment and restriction of chain mobility, respectively. The samples' improved rigidity accounted for the increased crystallinity by ZnO, which the nanofiller further reduced elongation at break. However, adding thymol improved the ductility of the blend nanocomposites. Despite the increased flexibility and crystallization properties, a common expectation is that some functional properties of host polymers, such as tensile strength and modulus, as well as the antibacterial activity, will decrease or remain unchanged with the addition of plasticizers, suggesting that nanofillers are needed to achieve the best balance of properties. Furthermore, it is recommended that the nanofillers act as compatibilizers in the ternary systems, and depending on their localization state, they can enhance the final properties (Taguet et al., 2014).

Recently, researchers have been using three-phase models to theoretically forecast the tensile strength and modulus of polymeric blend nanocomposites (Ghassemi et al., 2022). The ability to accurately predict the mechanical characteristics is required for using new nanocomposite materials in engineering design (Zamanian et al., 2021). By employing this computational technique in this study, we attempt to understand the structure–property correlations of different nanocomposites better, utilizing both experimental and theoretical methods. The present study aims to improve and balance PLA blend nanocomposites' crystallization, toughness, and antibacterial behavior in the simultaneous presence of ESO and ZnO NPs. We expect the results of this research to be attractive in the case of this important class of polymer nanocomposites applicable in the field of food packaging.

2. Curve fitting

The subsequent models can be employed to assess the mechanical characteristics of polymer blend nanocomposites, including their tensile modulus and strength:

2.1. Parallel or Voigt model

Using the mixing law and the isostrain condition, the Parallel or Voigt model determines an upper bound for the tensile modulus of a two-component system (Chow, 1980):

$$E_{II} = E_m\varphi_m + E_d\varphi_d \tag{1}$$

In this equation, E_{II}, E_m, and E_d express the modulus of the blend (or its nanocomposite), matrix, and dispersed phase, respectively. Furthermore, φ_m and φ_d represent the matrix and dispersed phase volume fractions, respectively.

2.2. Series or Reuss model

Unlike the parallel model, the series or Reuss model can predict the minimum value related to the modulus of a blend nanocomposite. This model can be achieved by utilizing the equation provided below (Ahmed and Jones, 1990):

$$E_{II} = \left[\left(\frac{\varphi_m}{E_m}\right) + \left(\frac{\varphi_d}{E_d}\right)\right]^{-1} \tag{2}$$

2.3. Guth model

This model can be employed for such blend nanocomposites, considering the ZnO aspect ratio represented by α (Guth, 1945):

$$\frac{E_{II}}{E_m} = 1 + 0.67\alpha\varphi_f + 1.62\left(\alpha\varphi_f\right)^2 \tag{3}$$

2.4. Halpin-Tsai model

Herman and Hill created this model to predict the modulus of unidirectional nanocomposite sheets (Fornes and Paul, 2003; Hill, 1964):

$$\frac{E_{II}}{E_m} = \frac{1 + 2\alpha\eta\varphi_f}{1 - \eta\varphi_f} \tag{4}$$

Where $\eta = (E_f/E_m - 1)/(E_f/E_m + 2\alpha)$ is the shape parameter associated with the geometric features of the filler.

2.5. Hui-Shia model

This model presupposes the existence of excellent interfacial bonding between the matrix and reinforcements (Dayma and Satapathy, 2010):

$$\frac{E_{II}}{E_m} = \left[1 - \frac{\varphi_f}{4}\left(\frac{1}{\zeta} + \frac{3}{\zeta + \Lambda}\right)\right]^{-1} \tag{5}$$

$$\zeta = \varphi_f + \frac{E_m}{E_f - fE_m} + 3\left(1 - \varphi_f\right)\frac{(1-g)\alpha^{-2} - \frac{g}{2}}{\alpha^{-2} - 1} \tag{6}$$

$$\Lambda = (1-\varphi_f)\left(\frac{3(\alpha^{-2}+0.25)g - 2(\alpha^{-2})}{\alpha^{-2}-1}\right) \quad (7)$$

Where $g = \alpha^{-1}\pi/2$.

2.6. Paul model

This model is controlled by the macroscopically uniform stress in the constituents of the nanocomposites (Paul, 1959):

$$\frac{E_{II}}{E_m} = \frac{1+(\frac{E_f}{E_m}-1)\varphi_f^{2/3}}{1+(\frac{E_f}{E_m}-1)(\varphi_f^{\frac{2}{3}}-\varphi_f)} \quad (8)$$

where E_f is tensile modulus of the nanofiller.

2.7. Maxwell model

The Maxwell model was developed mainly for nanocomposites with uniformly distributed fillers. The expression of this model is as follows (Ohama, 1987):

$$\frac{E_{II}}{E_m} = \frac{1+2\varphi_f(\frac{E_f}{E_m}-1)/(\frac{E_f}{E_m}+2)}{1-\varphi_f(\frac{E_f}{E_m}-1)/(\frac{E_f}{E_m}+2)} \quad (9)$$

2.8. Nielsen model

Nielsen modified the Halpin-Tsai theoretical model, which is shown below:

$$\frac{E_{II}}{E_m} = \frac{1+\chi\eta\varphi_f}{1-\eta\psi\varphi_f} \quad (10)$$

Where $\chi = 2.5(\alpha)^{0.645} - 1$ under the non-slippage condition (Rao, 2007). The parameter ψ relates to the maximum packing volume fraction (φ_M) of filler according to the following equation:

$$\psi = 1 + \left(\frac{1-\varphi_M}{{\varphi_M}^2}\right)\varphi_f \quad (11)$$

2.9. Pukanszky model

This model was formulated to calculate the tensile strength of nanocomposites in the following manner:

$$\sigma_{yc} = \sigma_{ym}\frac{1-\varphi_f}{1+2.5\varphi_f}\exp(\beta\varphi_f) \quad (12)$$

The symbols σ_{yc} and σ_{ym} represent the nanocomposite and matrix yield strengths, respectively. The parameter β is an empirical value that indicates the degree of interaction between the matrix and filler, specifically in terms of how efficiently the load is transferred between them (Dayma and Satapathy, 2010).

2.10. Nicolais and Narkis model

Nicolais and Narkis introduced the following formula for forecasting the tensile strength of nanocomposites for cubic matrix reinforced with uniformly distributed spherical particles (Narkis and Nicolais, 1971):

$$\sigma_{yc} = \sigma_{ym}\left(1 - 1.21\varphi_f^{\frac{2}{3}}\right) \quad (13)$$

3. Experimental

3.1. Materials and preparation

PLA (grade Ingeo 4043D), with a 1.21 g/cm^3 density, melting point of 145–160 °C, and molecular weight of 1,000,000 g/mol, was obtained from Nature Works Company, USA. Epoxidized soybean oil (ESO, ≥ 99.5%) containing an average of > 6 epoxy groups per molecule and a chemical formula of $C_{57}H_{98}O_{12}$ was obtained from Aladdin Industrial Corporation (Shanghai, China). ZnO powder, with an average particle size of <100 nm, was purchased from Sigma Aldrich (Germany).

Polylactic acid granules and zinc oxide nanoparticles were placed in an oven at 40 °C for 24h to dehydrate completely. In the first step, PLA, ESO, and ZnO with specific concentrations (Table 1) were blended via mechanical stirring in a well-washed beaker glass. The resulting mixture was kept in a closed container at room temperature for 24h. Afterward, each sample container was put in a laboratory's internal batch mixer with a capacity of 70 g at a temperature of 140 °C and 60 rpm for 15 min to ensure that the nanoparticles were evenly distributed throughout the polymer matrix. Finally, to achieve nanocomposite films with a thickness of 2 cm, all the samples were transformed into uniform film sheets using compression molding at a temperature of 140 °C and a pressure of 10 MPa. Each film follows the same procedures illustrated in Fig. 1.

3.2. Characterization

The chemical structure of each sample was investigated using Fourier Transform Infrared Spectroscopy (Bruker, Equinox 55, USA).

Using scanning electron microscopy (SEM) (TESCAN®, Czech Republic), the fracture surface of the samples was imaged to assess the morphological features. The localization of ZnO nanoparticles and their dispersion state in nanocomposite samples were investigated using energy-dispersive X-ray spectroscopy (EDS) from Oxford INCA®, UK.

The crystalline structures of nanocomposites were studied via X-ray diffraction analysis (XRD) through a Wide-Angle X-ray Scattering (WAXS) device (FK60-04 D5000, Siemens Co., Germany) operating at 40 kV and 20 mA. Cu Kα radiation (λ = 1.54 nm) was utilized with a detector that moved through 2θ = 5 to 40° and 2θ = 0.02°/sec. Moreover, the crystallinity index (CI) of the samples is calculated according to the following equation (Arshian et al., 2023):

$$X(\%) = \frac{A_c}{A_c + A_a} \times 100 \quad (14)$$

A_c and A_a represent the crystalline and amorphous areas, respectively. These data are generated using the Origin software.

Under a nitrogen environment, DSC (Mettler, Switzerland) was used to test the thermal characteristics of neat PLA and its blends. The specimens, which weighed around 5 mg before drying, were subjected to testing. Next, the specimens were rapidly heated from 0 to 190 °C at 10 °C per minute. After 5 min of heating, they were cooled to −50 °C at 10 °C per minute and kept at that temperature for 5 min to remove any thermal history. The second heating curve was used to measure the PLA's T_g, T_{cc}, ΔH_{cc}, T_m, and ΔH_m, which are the glass transition temperature, cold crystallization temperature, cold crystallization enthalpy, melting temperature, and melting enthalpy, respectively. The following

Table 1
The samples formulation.

Specimen	PLA (wt.%)	ESO (wt.%)	ZnO (wt.%)
PLA	100	0	0
100-1	100	0	1
100-3	100	0	3
100-5	100	0	5
95-5	95	5	0
90-10	90	10	0
80-20	80	20	0
90-10-1	90	10	1
90-10-3	90	10	3
90-10-5	90	10	5
80-20-1	80	20	1
80-20-3	80	20	3
80-20-5	80	20	5

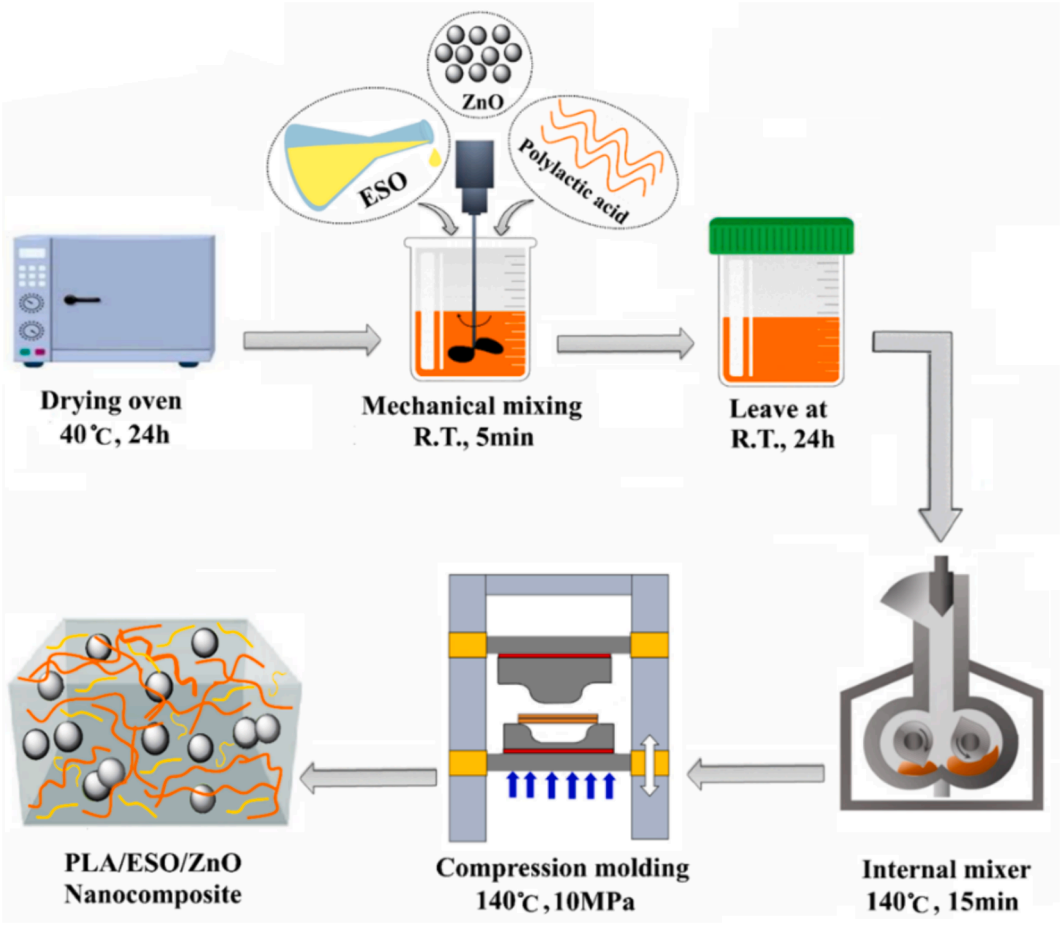

Fig. 1. Specimen preparation procedure.

is a calculation of the sample's PLA crystallinity (X_c, PLA) (Chen et al., 2015):

$$X_{c,PLA} = \frac{\Delta H_m - \Delta H_{cc}}{\Delta H_m^0} \times 100 \quad (15)$$

Where ΔH_m and ΔH_{cc} are the observed melting and cold crystallization enthalpy of PLA, respectively, and ΔH_m^0 is the theoretical melting enthalpy of 100% crystalline PLA (=93 J/g) (Xie et al., 2022).

The tensile properties of the rectangular-shaped specimens with a dimension of 5×3 cm were measured using a SANTAM-MTS20, Iran machine, according to ASTM D882-12. The testing speed was 10 mm/min, and a load cell of 6N was used at room temperature. Three separate tests took place, and the average results were recorded.

The contact angle of water and di-iodomethane was examined using a contact angle device (KRUSS G10, Germany) that employed the sessile drop method. Each sample underwent the test three times before reporting the average. Each amorphous film was tested by depositing five 4μL droplets of the testing liquid onto its surface. The picture of the droplet was taken 5 s after deposition to ensure that the liquid had reached thermodynamic equilibrium with the solid surface. Then, the samples' total surface free energy was determined by applying the Owens-Wendt technique (Żenkiewicz et al., 2009).

The nanocomposites' antibacterial properties were assessed using the disk diffusion method. Following impregnation with bacteria, the sample disks were positioned on the surface of Mueller-Hinton agar. After 24h of incubation at 37 °C, the inhibitory zone was examined on the plates.

The TGA instrument (Mettler Toledo) was used to conduct thermal stability studies in a nitrogen atmosphere at a heating rate of 10 °C/min.

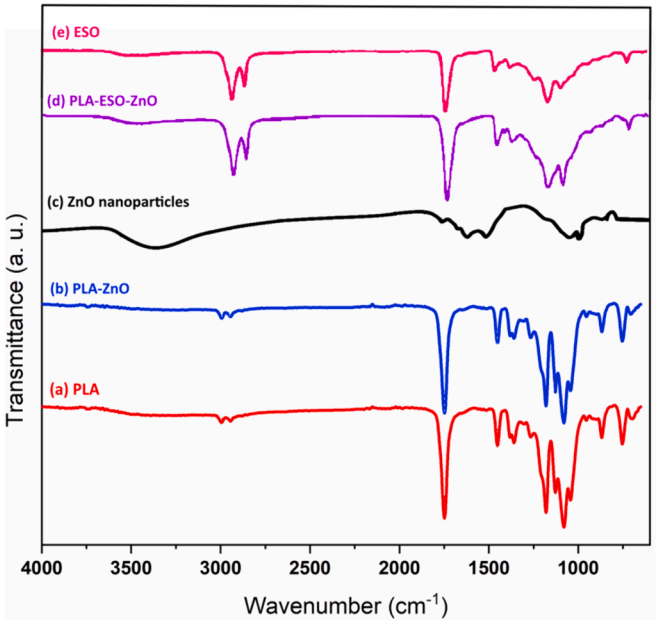

Fig. 2. FTIR spectra of the neat PLA, ZnO, PLA-ZnO, and PLA-ESO-ZnO.

4. Results and discussion

4.1. FTIR

Fig. 2 displays the FTIR spectra of PLA nanocomposites. In Fig. 2a, the surface hydroxyl groups of neat PLA are visible at 3450 cm^{-1}. The absorbances at 2946 and 2992 cm^{-1} indicate the presence of methyl groups in the PLA side chain, corresponding to the stretching vibration of C–H bonds (Jafari et al., 2022). The absorption band at 1748 cm^{-1} is also mainly due to the stretching of the C=O bond in the ester group. Moreover, the peaks at 1451 and 1370 cm^{-1} are caused by symmetric and asymmetric C–H stretching vibrations, whereas the absorptions at 1045–1267 cm^{-1} are related to the C-O stretching vibration (Chen and Zhen, 2021). For neat ZnO nanoparticles (Fig. 2c), the peak observed between 480 and 420 cm^{-1} corresponds to the stretching mode of Zn-O (PP, 2020). As is clear, the addition of ZnO did not alter any of the PLA peaks, except for a slight decrease in the intensity of the peak at 3450 cm^{-1} (Fig. 2b). This reduction indicates the formation of secondary forces, such as weak hydrogen bonds, between PLA and ZnO NPs. Fig. 2e shows that ESO has a distinct epoxy functional group structure, indicated by two peaks at 833 and 726 cm^{-1} (Litke et al., 2023). In addition, the peaks at 1157 and 1738 cm^{-1} were due to the C-O stretching and C=O (carbonyl) stretching of ester groups, respectively (Kumar et al., 2017). The displacement of these peaks in the blended nanocomposites demonstrates the potential interactions between components. Similarly, the peaks at around 2923 and 2840 cm^{-1}, which belong to the stretching vibration of aliphatic C–H stretching in ESO, are observed in another position in the PLA-ESO-ZnO (Fig. 2d), indicating the likelihood of hydrogen bonding with the ESO's oxirane group, the hydroxyl group of PLA, and the ZnO terminal (Han et al., 2020).

4.2. SEM-EDS

Figs. 3-7 depict the cryo-fractured surfaces of neat PLA, PLA-ZnO, and PLA-ESO-ZnO blend nanocomposites as detected by SEM-EDS. Based on the observations, the fractured surface of pure PLA exhibited a smooth and consistent appearance (Fig. 3). However, adding 3 wt% of ZnO NPs resulted in roughness on the PLA surface, suggesting the presence of a more complex fracture propagation route while maintaining a uniform distribution, except for specific clusters of the ZnO NPs, as shown by white dots in Fig. 4b) (Shankar et al., 2018). It is well known that good inter-component interactions and the formation of secondary forces, such as hydrogen bonds between the PLA polymer and ZnO, cause good dispersion of the nanoparticles (Kim et al., 2019; Tan et al., 2023; Yu et al., 2021).

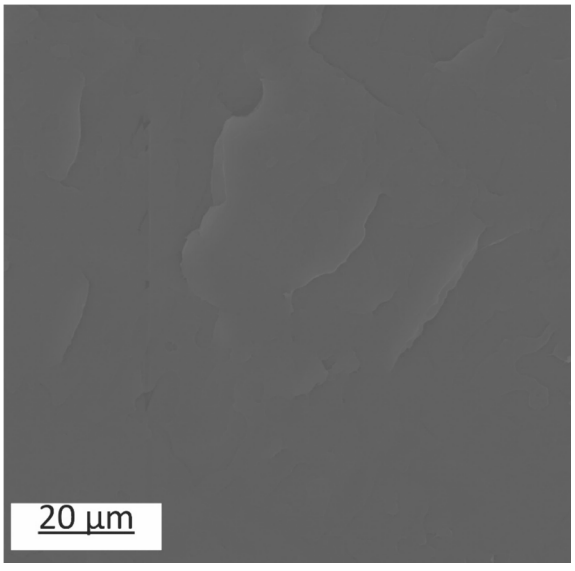

Fig. 3. SEM image of the neat PLA.

Upon blending with 5 wt% of ESO, the blended nanocomposites exhibited spherical holes on their cracked surfaces (Fig. 5), showing the matrix-droplet structure (Silverajah et al., 2012). In the case of the 90–10-5 blend nanocomposites, there was a significant reduction in the diameter and number of holes. These results validate that adding more ZnO NPs enhanced the compatibility between PLA and ESO, indicating the presence of robust contact forces between PLA, ESO, and ZnO. In other words, ZnO has prevented the coalescence phenomenon and enhanced the characteristics at the interface (Díez-Pascual and Diez-Vicente, 2014; Rokbani and Ajji, 2018; Tayouri et al., 2022). Moreover, ZnO increases the viscosity of the PLA-ESO system, and at the same shear rate, the increased shear stress can cause smaller ESO droplets within the matrix (Jalalifar et al., 2020). Fig. 7 shows that the morphological structure of the blend nanocomposite is greatly affected by the addition of 20 wt% ESO. PLA underwent morphological modifications because of the increased ESO (as a low-molecular-weight phase) concentration, transitioning from brittle to ductile fracture. A similar discovery can be found in the literature (Raghunath et al., 2018).

4.3. XRD results

The microstructure and crystallinity properties of sample films were analyzed using XRD patterns in Fig. 8. Fig. 8a displays a broad diffraction peak, from 2θ=15.0° to 20.0°, which arises from the inherent amorphous structure of the PLA (Arshian et al., 2023; Paydayesh et al., 2022). Upon mixing with ESO, no bulge shifting observation indicates no changes in the corresponding interlayer spacing in PLA structure (Fig. 8b and 8c) (Giita Silverajah et al., 2012). Besides, no discernible crystalline peaks occur, accounting for the substantial interactions between the PLA O–H group and the epoxy group of ESO through hydrogen bonding (Raghunath et al., 2018; Jian et al., 2017). Fig. 9 depicts the most feasible interactions that dominate the system.

The 90–10-1 nanocomposite film shows a clear crystallization peak near 2θ of approximately 16.5°. This peak corresponds to the diffraction of the (200)/(110) planes of the typical orthorhombic PLA crystal, similar to previous findings in the literature (Pantani et al., 2013; Wu and Wu, 2006). In addition, the planes (100), (002), (101), (102), (110), (103), (200), (112), and (201) of the hexagonal crystal of ZnO NPs are corresponded to the distinctive peaks at 2θ = 31.6, 34.4, 36.2, 47.4, 56.7, 62.7, 66.2, 67.9, and 69.0°, respectively (Agrawal et al., 2010). As confirmed, an increase in the amount of ZnO leads to a decrease in the intensities of the crystalline peak at a 2θ of about 16.5°. However, the presence of the ZnO NPs enhanced the total crystallinity of the blended nanocomposites from 9.5 for 90–10-1 to 11.3% for 90–10-5. The comparison of Fig. 8d and 8e indicates that a lower concentration of ZnO (as a nucleation agent) can lead to improved arrangement of PLA chains. This ordered structure of PLA occurs because the interactions between PLA and ESO chains are interrupted by weak hydrogen bonds formed between the ZnO and the PLA polymer matrix (Tan et al., 2023). Nevertheless, the PLA chain will be entrapped at the higher level of ZnO, leading to lower intensities of the PLA characteristic peaks (Shankar et al., 2018; Murariu et al., 2011; Jayaramudu et al., 2014).

4.4. DSC results

DSC was used to investigate the thermal properties of neat PLA and PLA-ESO-ZnO blend nanocomposites (Fig. 10 and Table 2). It is observed that the addition of ESO reduced the T_g values of blend nanocomposites. The plasticizer increased chain mobility by replacing the interaction between the original PLA chains, leading to a lower T_g (Wang et al., 2021; Ebadi-Dehaghani et al., 2015; Lee et al., 2003). Moreover, the T_g of PLA-ESO blends decreased when 5 wt% of ZnO was added to the mixtures. This behavior can be associated with the catalytic effect of the

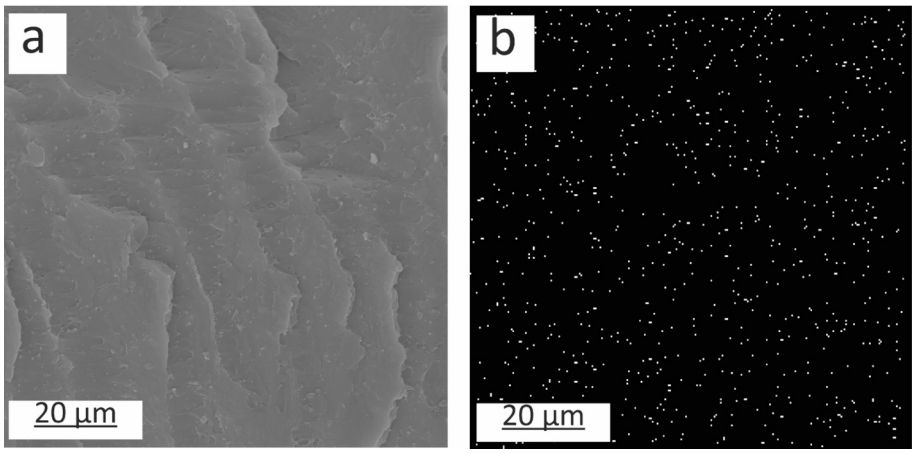

Fig. 4. a: SEM and b: ESD images of the PLA containing 3 wt% of ZnO.

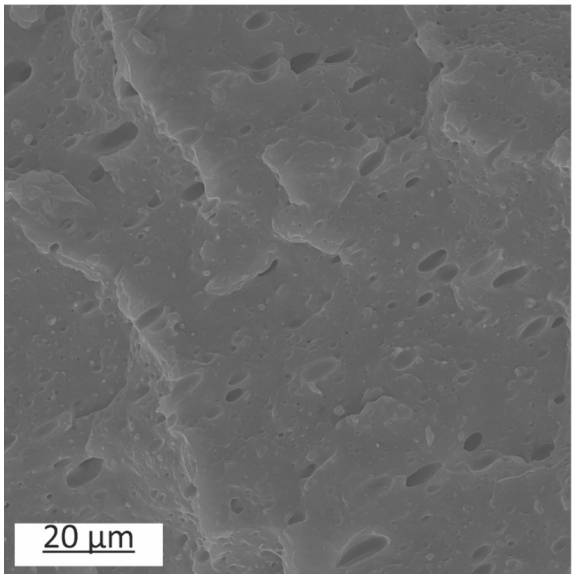

Fig. 5. SEM image of the 95–5 blend containing 3 wt% of ZnO.

ZnO NPs on the PLA chain's degrading reaction, consistent with the findings in the literature (Anžlovar et al., 2018; Lizundia et al., 2019).

As evident, the ZnO did not positively affect the crystallization of the 90–10 blend. Although NPs can increase crystallization rates as nucleating agents, they can also slow down spherulite development by restricting the order of polymer chain segments and raising the T_{cc} value (Kim et al., 2019; Quiles-Carrillo et al., 2018). The 90–1-5 has lower values of ΔH_{cc} than 90–10-1, which might indicate less conversion of amorphous regions into crystalline domains (Agbakoba et al., 2023). On the other hand, 80–20-5 blend nanocomposites had higher crystallinity and a lower ΔH_{cc} than other samples. The crystallite's quality is responsible for such contrary results (Kaczor et al., 2022). PLA-ESO has a comparatively low T_g, accompanied by a reduction in T_{cc} as ESO increases in the blended nanocomposites (Chu et al., 2017). As a result, the spherulitic growth rate of PLA-ESO-ZnO improves with decreasing PLA content and increasing the ZnO concentration (Han et al., 2017; Farrag et al., 2022).

As indicated, the T_m of PLA marginally decreases with the addition of ESO and ZnO (Table 2). In simple terms, the reduced melting point results from the increased mobility of the polymer chains facilitated by plasticizers and nanofillers (Chapple et al., 2013; Diep et al., 2019). This section showed that increasing NPs to higher levels (about 5 wt%) had a better nucleation effect on the 80–20 blend nanocomposites than the 90–10 matrix. These specific results are highly dependent on the quality of the crystals and morphological features. Fig. 11 illustrates the intermolecular interactions of the components with each other, in which ZnO NPs play the role of compatibilizers and nucleation agents.

4.5. Tensile properties

Tensile tests are used to study the influence of ESO and ZnO on PLA's mechanical properties, and the resulting data are shown in Table 3 and Figs. 12–15. The tensile strength and modulus of PLA decreased with the addition of ESO, demonstrating its plasticizer effect (Fig. 12). Generally, plasticizers disrupt the intermolecular interactions between polymer chains, resulting in lower chain cohesion and strength (Darie-Niță et al., 2016). When ESO and PLA are blended, they can become partially miscible, dissolving the connection sites and weakening the forces between the ESO fatty chains. Consequently, phase separation for ESO would be improved (Khoo and Chow, 2017). In this regard, we can see that the blend with 10 wt% ESO was more rigid in structure and had a different effect on lowering the tensile modulus of the PLA compared to those with 5 and 20 wt% plasticizer. As can be seen, the blend 90–10 significantly increased (141.4%) in elongation-at-break compared to neat PLA, indicating that ESO improved the flexibility and mobility of PLA chains. At the initial stage of ESO loading, PLA's elongation-at-break increased dramatically, then decreased continuously. This can be attributed to poor phase separation of ESO and their weak interactions with the PLA matrix when ESO content exceeded 10 wt% (Zhao et al., 2012).Fig. 16..

According to Fig. 13, introducing ZnO at 1 wt% decreased the tensile strength and modulus of the PLA. However, As the amount of ZnO NPs increased, the tensile modulus improved, while the tensile strength peaked at 3 wt% of the NPs due to enhanced filler-matrix interactions (Ahmed et al., 2016; Tayouri et al., 2023). As expected, when ZnO was added to PLA film, the elongation-at-break value dropped from 16% for neat PLA to 3.4% for PLA containing 5 wt% ZnO. The chain entanglement effect causes this phenomenon.

We witness that the tensile strength and modulus of the blended nanocomposites improved as the rigid ZnO content increased, creating a better loading and stiffening physical network. Besides, adding 5 wt% of ZnO nanoparticles in PLA-ESO-ZnO films enhanced ductility since ZnO NPs, with their high aspect ratio, were uniformly dispersed in the matrix and entrap the polymeric chains (Jayaramudu et al., 2014; Hocker et al., 2018). As a result, the packing mode of the ordered PLA structure was reduced, and elongation at break will increase. In addition, there is speculation that this behavior is likely linked to the polylactic acid matrix degradation during melt mixing, which could be caused by the catalytic action of ZnO (Quiles-Carrillo et al., 2018; Keshavarzi et al., 2019). Another contributing factor might be the enhancement of ZnO

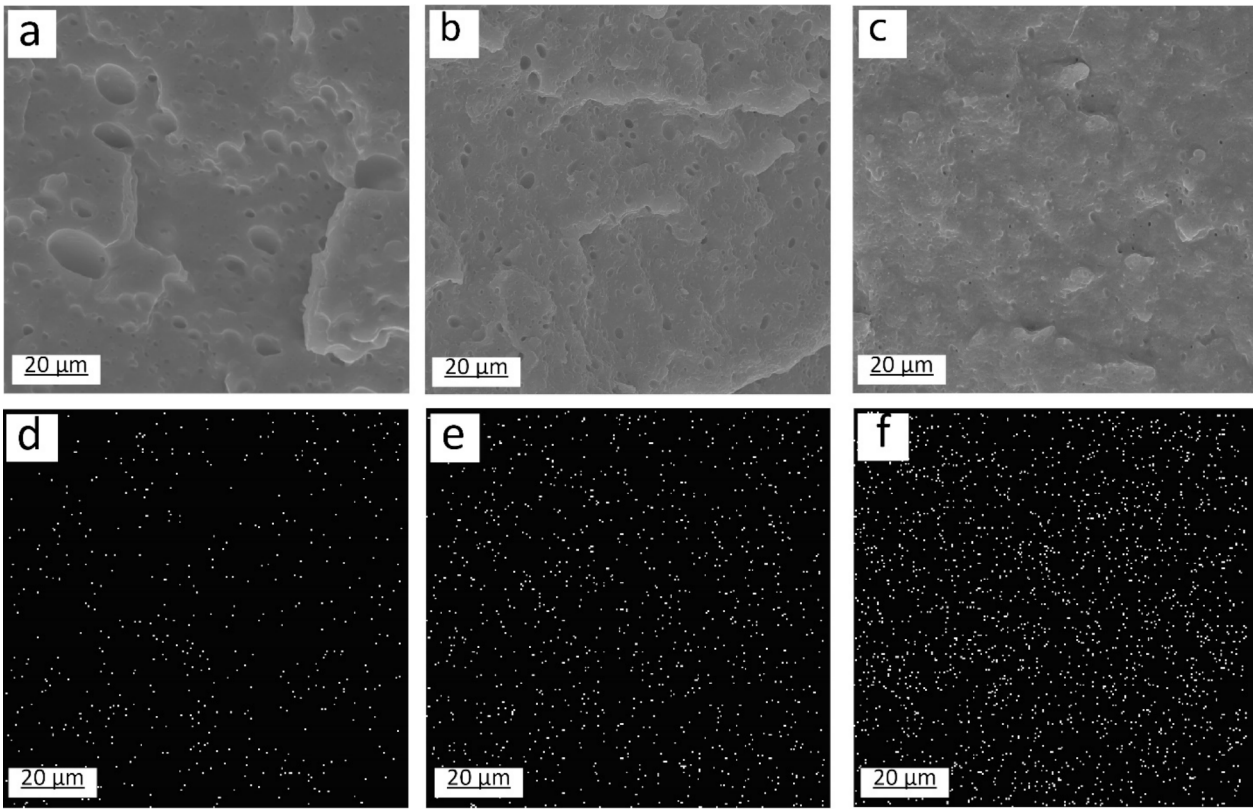

Fig. 6. SEM-EDS images of the a-d: 90–10-1, b-e: 90–10-3, and c-f: 90–10-5.

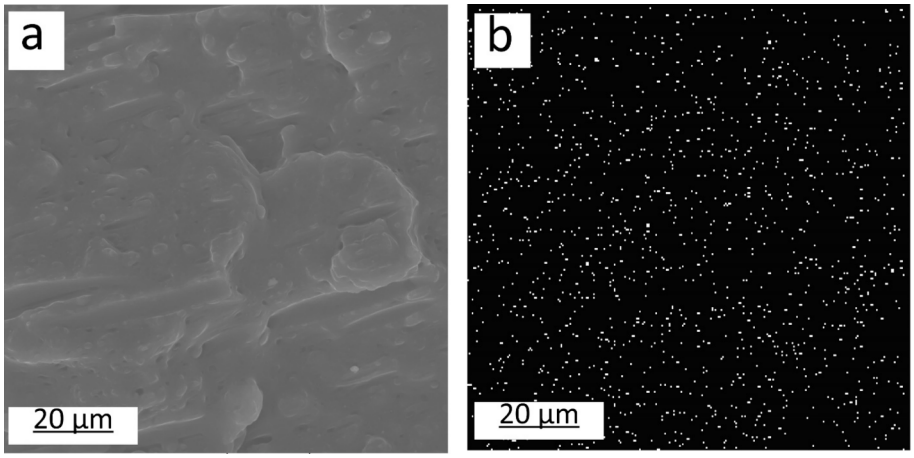

Fig. 7. SEM and EDS images of the 80–20 blend containing 3 wt% of ZnO.

content, which improved the morphology of ESO within the PLA matrix and increased chain mobility. Ultimately, due to fine structural features, the 90–10-5 sample shows the highest strength, modulus, and elongation-at-break (about 35%) properties among all samples (Mauck et al., 2016).

The tensile modulus of the PLA-ESO-ZnO blend nanocomposites was determined using experimental data and Equations (1)–(11). The obtained findings were compared against each other, revealing that the Maxwell, Paul, and Hui-Shia models offer more accurate predictions for the 90–10-ZnO. Even though the Maxwell equation accurately predicts the experimental findings, the Paul and Hui-Shia models yield better when the nanoparticle content is higher. As for the 80–20-ZnO blend, the best prediction can be derived from the upper model for lower nanoparticle content, whereas the Paul and Halpin-Tsai models are suitable for higher loadings.

As illustrated in Fig. 17, the tensile strengths of the nanocomposites were determined using the models proposed by Pukanszky (Equation (12) and Nikolais and Narkis (Equations (13). The 90–10-ZnO and 80–20-ZnO nanocomposites' empirical β parameters were found by comparing the experimental data with the Pukanszky model, assuming that σ_{ym} is the tensile strength of the blend nanocomposites. The β parameter value is affected by several variables, including the nanofiller's average size, the interface strength between the polymer and nanofiller, and the average contact area between the components. These variables impact the nanocomposite's load-bearing ability, and the higher value of β will cause the curve associated with the Pukanszky equation to move to a larger σ_{yc}. Compared to the Nikolais and Narkis model, the Pukanszky model yields more precise predictions of the

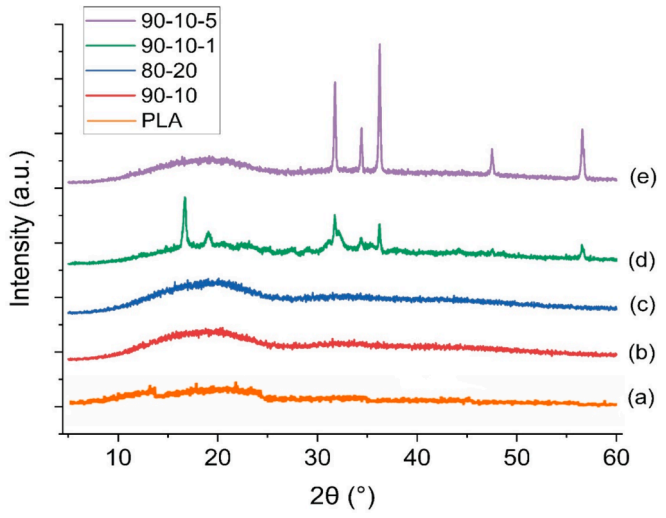

Fig. 8. XRD pattern of the PLA samples.

tensile strengths.

4.6. Contact angle and antibacterial properties

The Owens-Wendt method was used to calculate the total surface-free energies of the nanocomposites. Accordingly, the contact angles of each sample were measured against polar solvent (water) and nonpolar solvent (diiodomethane) (Thanakkasaranee et al., 2018). Table 4 summarizes the resulting data. The neat PLA sheet has a water contact angle of 63.969°, while adding 3 wt% of ZnO increased the water contact angle by 1.9°, suggesting an enhancement in the PLA's hydrophobicity and surface roughness (Li et al., 2021; Yang et al., 2012; Mora-Fonz et al., 2017). This observation can be attributed to the interactions between ZnO nanoparticles and the hydrophilic groups on PLA chains (Ismail et al., 2022). The results also show that adding plasticizer to the blend nanocomposites enhanced their hydrophilicity and increased total surface energy due to polar groups such as oxirane in ESO (Aydın et al., 2017; Meadows et al., 2018). Fig. 18 indicates that the 90–10-3 has comparatively lower contact angles than 80–20-3 blend nanocomposites.

The effect of increasing ZnO content on the contact angle measurements of the 90–10 blend is illustrated in Fig. 19. The figure indicates that adding ZnO NPs to the blend can increase the contact angles of water and diiodomethane and reduce both polar and dispersive surface energies due to the low molecular interactions of non-London (dipole–dipole) and London dispersion forces, respectively (Zhuang and Hansen, 2009). It can be stated that the crystalline domains caused by the presence of the ZnO NPs can block the access of water molecules to the hydrophilic groups of the polymer components (Arshian et al., 2023; Hosseinvand et al., 2022).

The PLA materials' antibacterial abilities against Gram-positive (S. aureus) and Gram-negative (E. coli) were studied using the disk diffusion method. The obtained results are shown in Fig. 20 and Table 5. As can be seen, PLA materials had no antibacterial activity against E. coli, indicating the structural distinction of the bacteria's cell walls, which was emphasized in the literature (Espitia et al., 2012; Mizielińska et al., 2018). Another difference between E. coli and S. aureus is how much negative charge is on their membranes. S. aureus with less negative charge interacts more strongly with the negatively charged ROS

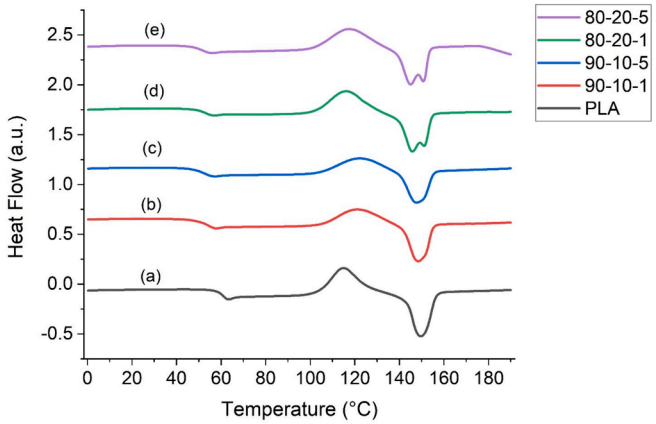

Fig. 10. DSC curves of the samples.

Table 2
Thermal properties of the PLA samples.

Sample	T_g (°C)	T_{cc} (°C)	ΔH_{cc} (j/g)	T_m (°C)	ΔH_m (j/g)	X_c (%)
PLA	61.1	114.7	24.8	149.6	25.2	0.42
90-10-1	54.3	120.9	21.7	148.6	19.4	2.45
90-10-5	52.5	122.0	19.2	147.8	18.3	0.9
80-20-1	53.0	116.2	26.3	145.8	23.8	2.67
80-20-5	51.8	117.3	25.8	144.9	22.8	3.2

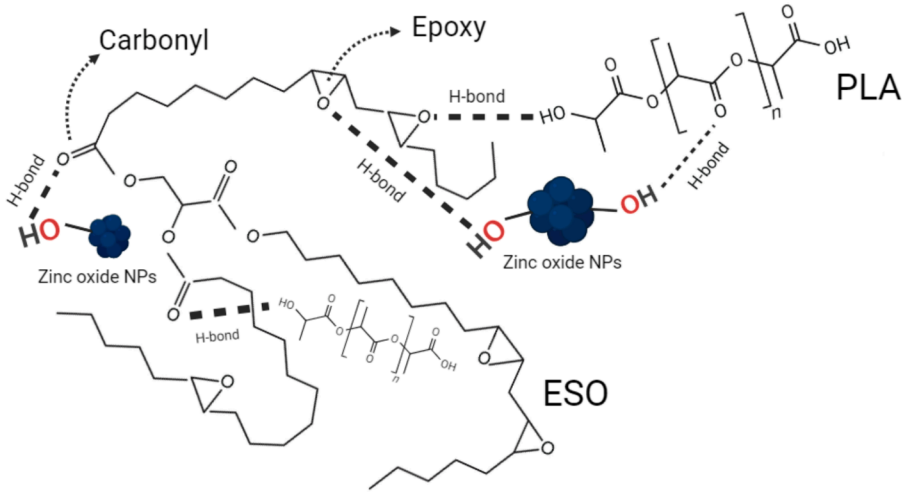

Fig. 9. The possible interactions between the components of the PLA-ESO-ZnO blend nanocomposites.

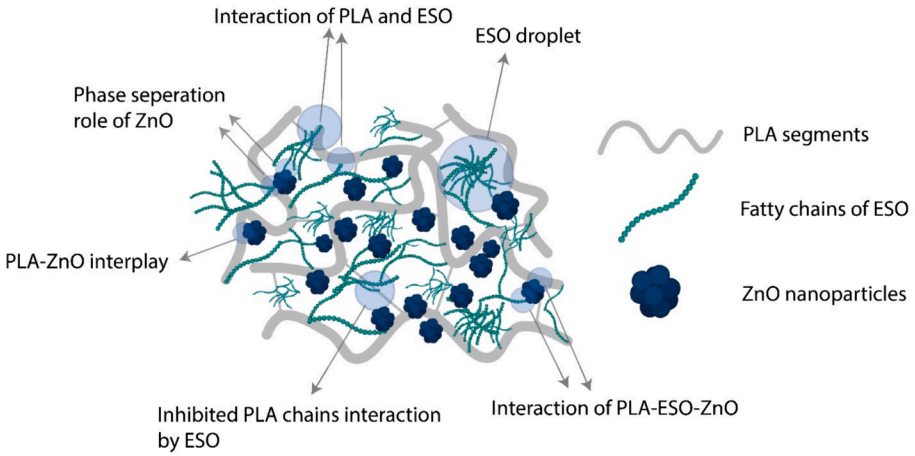

Fig. 11. Possible interaction mechanisms of PLA-ESO-ZnO blend nanocomposites.

Table 3
Mechanical properties of the samples.

Sample	Yield strength (MPa)	Tensile modulus (MPa)	Elongation-at-break (%)
PLA	40.68 ± 0.9	682.00 ± 32	16 ± 4.2
95-5	28.02 ± 1.1	461.93 ± 25	34.2 ± 3.1
90-10	24.20 ± 0.8	527.99 ± 19	157.4 ± 12.5
100-1	35 ± 1.3	446 ± 29	8.9 ± 1.7
100-3	36 ± 1.0	753 ± 35	4.7 ± 1.9
100-5	30 ± 1.5	883 ± 52	3.4 ± 0.4
90-10-1	17.96 ± 1.2	598.10 ± 17	6.49 ± 1.0
90-10-3	22.95 ± 1.4	676.07 ± 29	5.9 ± 0.7
90-10-5	27.88 ± 1.1	895.26 ± 26	35 ± 1.2
80-20	23.52 ± 1.5	203 ± 27	20 ± 4.4
80-20-1	12.46 ± 0.7	469 ± 31	5.1 ± 0.8
80-20-3	17.167 ± 1.2	618 ± 41	11 ± 1.6
80-20-5	24.59 ± 0.5	778 ± 39	33 ± 2.8

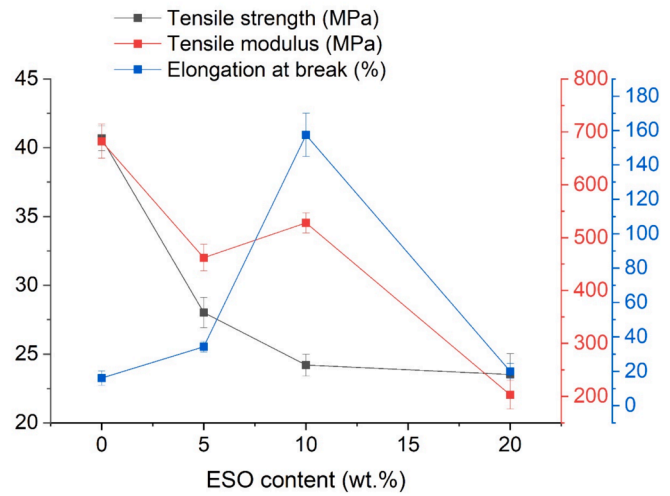

Fig. 12. Effect of ESO on the mechanical properties of the neat PLA.

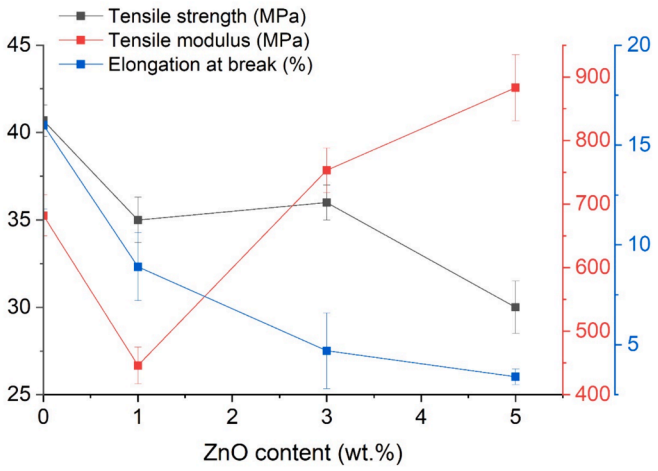

Fig. 13. Effect of ZnO on the mechanical properties of the neat PLA.

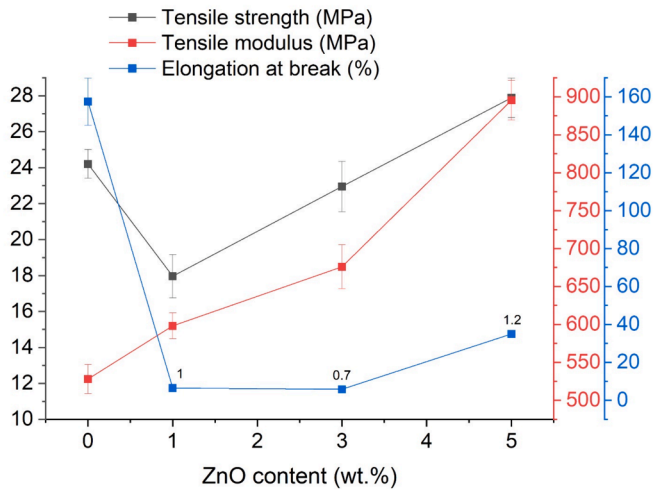

Fig. 14. Effect of ZnO content on the 90–10 blend nanocomposites.

(reactive oxygen species) in the ZnO NPs' antibacterial mechanism (Zhang et al., 2017). As depicted, the ESO had no significant effect on the antibacterial properties of the PLA. The 90–10-5 blend nanocomposite showed a prominent antibacterial circle, revealing the highest inhibitory ability of about 6 mm against S. aureus. Indeed, zinc ions impede bacterial development and damage the microbial surface (Shankar and Rhim, 2019; Restrepo et al., 2019). These findings suggest that, in terms of food preservation, the produced materials are

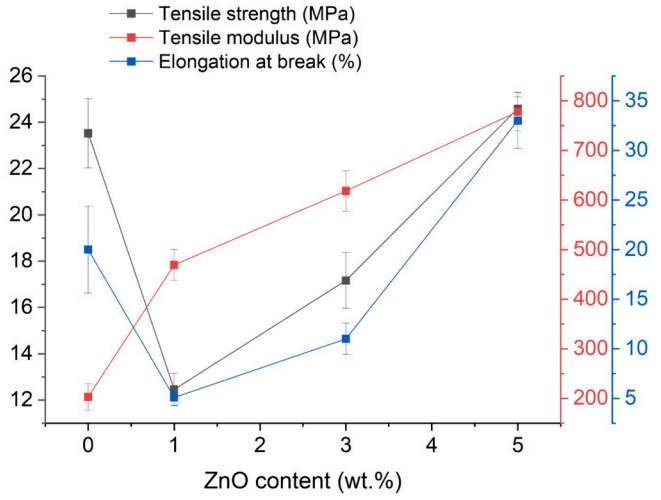

Fig. 15. Effect of ZnO content on the 80–20 blend nanocomposites.

Table 4
Contact angles and surface free energies of neat PLA and its blend nanocomposites.

Sample	Water contact angle (°)	Diiodomethane contact angle (°)	Polar part (mN/m)	Disperse part (mN/m)	Total surface free energy (mN/m)
PLA	63.969	29.67	8.23	47.27	55.50
100-3	65.917	18.705	6.97	48.15	55.12
95-5-3	65.921	19.119	7.00	48.04	55.04
90-10	61.421	11.818	8.55	49.73	58.28
90-10-1	63.345	12.808	7.74	49.55	57.29
90-10-3	62.175	14.194	8.34	49.26	57.60
90-10-5	63.678	22.792	8.69	46.91	55.61
80-20-3	57.697	9.587	10.20	50.09	60.30

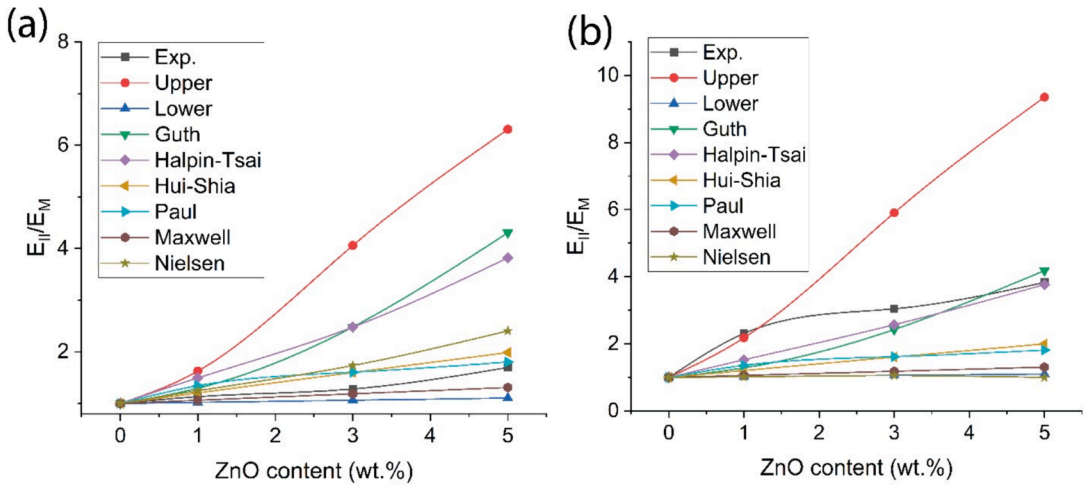

Fig. 16. Comparison between the experimental and theoretical tensile modulus of (a) 90–10-ZnO and (b) 80–20-ZnO nanocomposites.

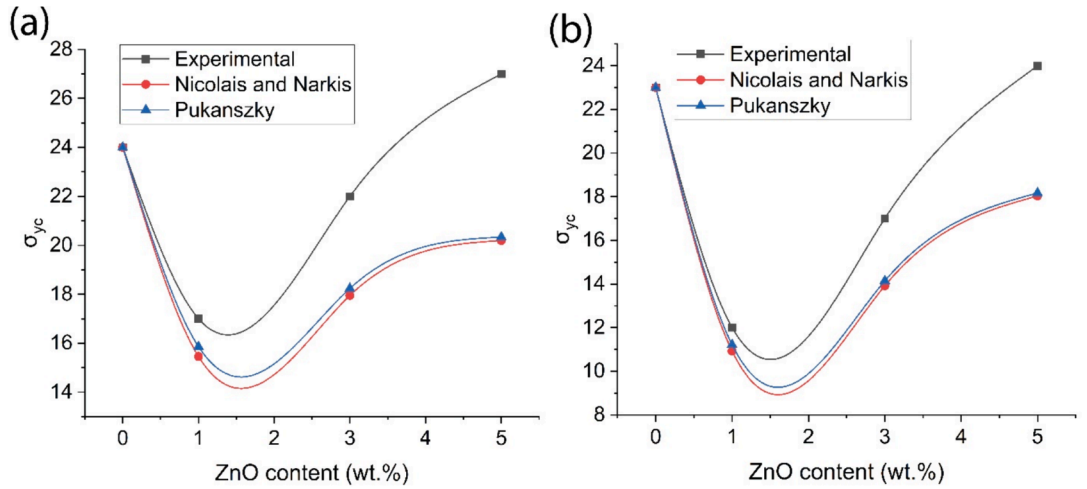

Fig. 17. Comparison between the experimental data and theoretical tensile strengths of (a) 90–10-ZnO and (b) 80–20-ZnO nanocomposites.

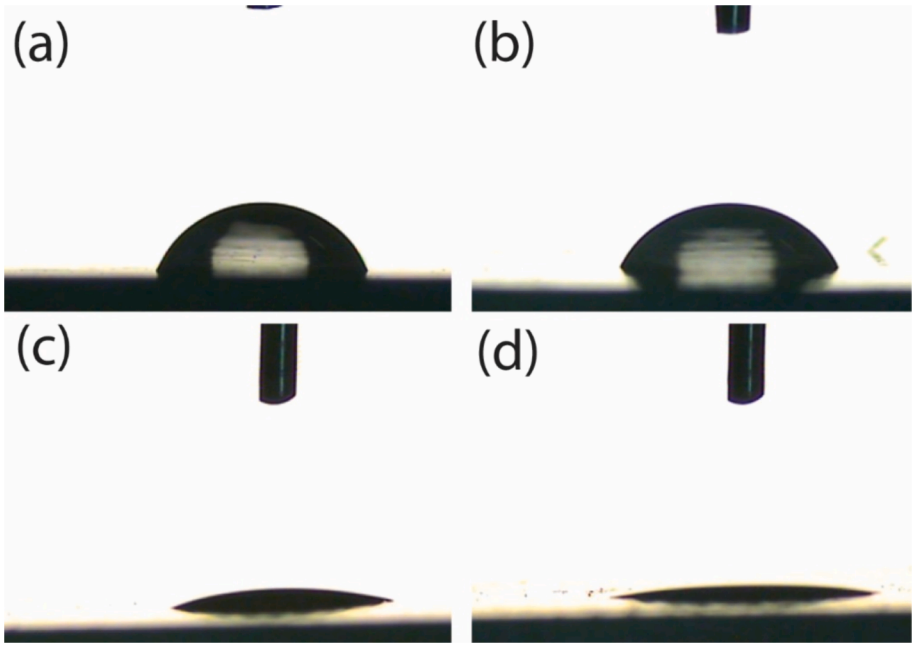

Fig. 18. Contact angle analysis of (a) and (b) for water and (c) and (d) for diiodomethane of 90–10-3 and 80–20-3 blend nanocomposites, respectively.

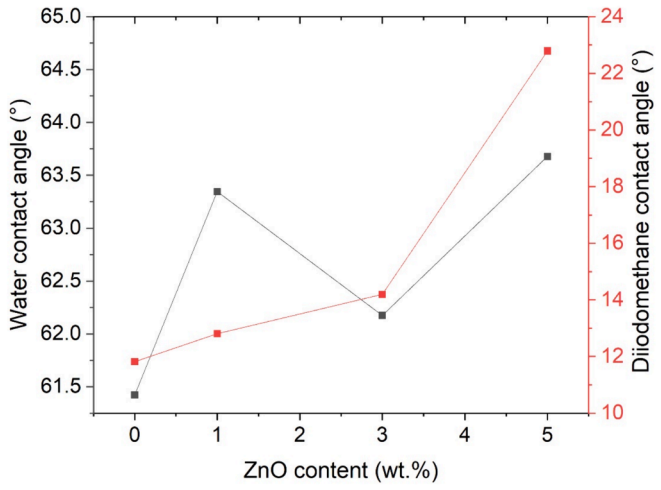

Fig. 19. Contact angle analysis of the 90–10 blend containing different ZnO content.

appropriate for use in food packaging applications.

4.8. TGA results

TGA was performed to determine the thermal stability of the 90–10 blend nanocomposites (as a candidate sample) in Fig. 21, and Table 6 presents the results comparing the thermal parameters, such as temperature at the initial stage (T_i) and maximum degradation temperature (T_{max}). As the temperature increased, the neat PLA exhibited a T_i of 265.9 °C and a T_{max} of 353.1 °C, which increased to 275.8 and 358.3 °C, respectively, once ESO was blended with the PLA matrix. In addition to the stabilizer effect of the ESO (Burkov et al., 2021), the interfacial interaction between PLA and ESO can lead to lower thermal decomposition of PLA's molecular chain (Zhao et al., 2021; Mahmud et al., 2019).

It is shown that the thermal degradation of the 90–10-1 blend nanocomposites started at higher temperatures than in neat polymer blends. This indicates that ZnO NP layers make the polymers more thermally stable by creating a more tortuous path within the polymeric matrix and blocking the movement of heat and gases (Pantani et al., 2013). Moreover, the presence of the ZnO improved the compatibility of the PLA and ESO, making the blends more resilient against thermal decomposition (Lim et al., 2019). However, adding 5 wt% of ZnO led to lower thermal stability of the blend nanocomposites. The reduction in thermal stability can be related to the catalytic activity of ZnO on the plyometric matrix at high temperatures. Other studies have also reported a similar observation, showing that ZnO NPs in PLA lead to less thermally stable materials. Among the investigated samples, the PLA-ESO-ZnO (90–10-1) blend exhibited the maximum values of T_i (365.3 °C) and T_{max} (425.1 °C), respectively.

5. Conclusion

Epoxidized soybean oil (ESO) has been used as a plasticizer in polylactic acid (PLA)-zinc oxide (ZnO) nanocomposites. The study discovered a competing influence of ZnO and ESO on the crystallization and ductility of PLA. ZnO NPs served as a nucleating agent and increased the strength of the matrix. At the same time, 10 wt% of ESO enhanced the chain mobility and elongation at the break of the neat PLA by 141.4%. However, the mechanism of the ZnO and ESO in simultaneous presence increases the crystallization behavior of the PLA and needs further studies. According to the structural analyses, adding ZnO establishes intermolecular solid interactions between components and positively affects the droplet size of ESO. The mathematical curve-fitting method showed an agreement with the tensile experimental findings. Unlike the ESO, adding more ZnO NPs in the PLA-ESO resulted in increased film thickness, improved contact angle, and antibacterial properties. Although the ZnO had a catalyst impact on the thermal decomposition of the PLA chains, the maximum degradation temperature (T_{max}) of the 90–10 blend increased by 66.8 °C as 1 wt% of the ZnO was added to the neat blend. These formulations based on PLA-ESO-ZnO blend nanocomposites are promising materials that can be prepared through currently used processing technology in the food packaging application with balanced and improved crystallization rate, toughness, antibacterial properties, and thermal stability.

CRediT authorship contribution statement

Mina Ghoroghi: Writing – original draft, Methodology,

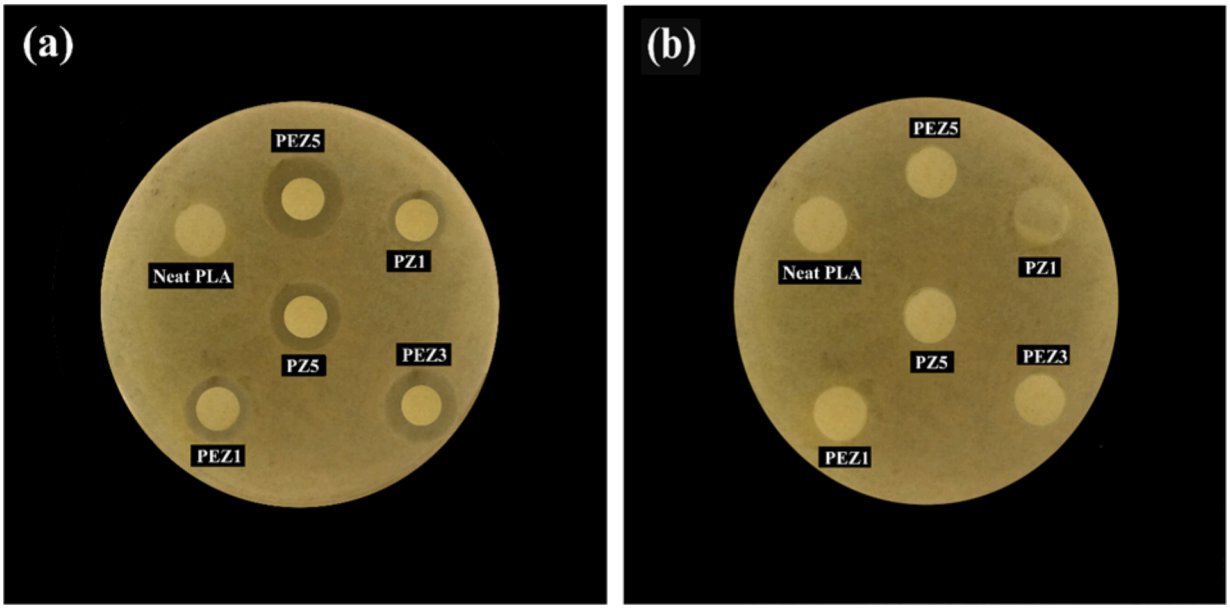

Fig. 20. Disk diffusion test against (a) Staphylococcus aureus and (b) Escherichia coli.

Table 5
Calculated zone of inhibition against S. aureus.

Sample code	*S. aureus*
PLA	0
PZ (100-1)	1
PZ (100-5)	3
PEZ (90-10-1)	2
PEZ (90-10-3)	4
PEZ (90-10-5)	6

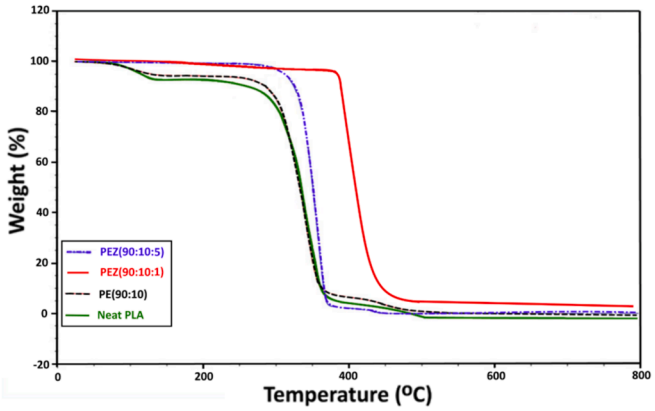

Fig. 21. TGA curves of PLA blend nanocomposites.

Table 6
Data was obtained from the TGA test for different samples.

sample	T_i (°C)	T_{max} (°C)
Neat PLA	265.9	353.1
PE (90:10)	275.8	358.3
PEZ (90:10:1)	365.3	425.1
PEZ (90:10:5)	297.0	389.5

Investigation, Data curation, Conceptualization. **Sara Estaji:** Writing – original draft, Methodology, Investigation, Formal analysis, Conceptualization. **Mohammad Iman Tayouri:** Writing – original draft, Validation, Software, Formal analysis, Conceptualization. **Reza Jahanmardi:** Writing – original draft, Supervision, Resources, Methodology, Investigation, Funding acquisition, Conceptualization. **Marcos A.L. Nobre:** Visualization, Supervision, Software, Funding acquisition. **Hossein Ali Khonakdar:** Writing – review & editing, Visualization, Project administration, Funding acquisition.

Declaration of competing interest

The authors declare that they have no known competing financial interests or personal relationships that could have appeared to influence the work reported in this paper.

Data availability statement

The data that support the findings of this study are available from the corresponding author upon reasonable request.

References

Agbakoba, V.C., Webb, N., Jegede, E., Phillips, R., Hlangothi, S.P., John, M.J., 2023. Mechanical Recycling of Waste PLA Generated From 3D Printing Activities: Filament Production and Thermomechanical Analysis. Macromol. Mater. Eng. 2300276.
Agrawal, M., Gupta, S., Zafeiropoulos, N.E., Oertel, U., Häßler, R., Stamm, M., 2010. Nano-level mixing of ZnO into poly (methyl methacrylate). Macromol. Chem. Phys. 211 (17), 1925–1932.
Ahmed, J., Arfat, Y.A., Castro-Aguirre, E., Auras, R., 2016. Mechanical, structural and thermal properties of Ag–Cu and ZnO reinforced polylactide nanocomposite films. Int. J. Biol. Macromol. 86, 885–892.
Ahmed, S., Jones, F., 1990. A review of particulate reinforcement theories for polymer composites. J. Mater. Sci. 25, 4933–4942.
Anžlovar, A., Kržan, A., Žagar, E., 2018. Degradation of PLA/ZnO and PHBV/ZnO composites prepared by melt processing. Arab. J. Chem. 11 (3), 343–352.
Arshian, M., Estaji, S., Tayouri, M.I., Mousavi, S.R., Shojaei, S., Khonakdar, H.A., 2023. Poly (lactic acid) films reinforced with hybrid zinc oxide-polyhedral oligomeric silsesquioxane nanoparticles: Morphological, mechanical, and antibacterial properties. Polym. Adv. Technol. 34 (3), 985–997.
Aydın, R.S.T., Akyol, E., Hazer, B., 2017. Influence of soybean oil blending with polylactic acid (PLA) films: in vitro and in vivo evaluation. J. Am. Oil Chem. Soc. 94 (3), 413–424.
Burkov, A., Kraev, A., Grishin, M., Vesnin, R., Fomin, S., Iordanskii, A., 2021. Structural features and properties' characterization of polylactic acid/natural rubber blends with epoxidized soybean oil. Polymers 13 (7), 1101.
Chapple, S., Anandjiwala, R., Ray, S.S., 2013. Mechanical, thermal, and fire properties of polylactide/starch blend/clay composites. J. Therm. Anal. Calorim. 113, 703–712.
Chausali, N., Saxena, J., Prasad, R., 2023. Nanotechnology as a sustainable approach for combating the environmental effects of climate change. J. Agric. Food Res. 12, 100541.

Chen, D., Zhen, W., 2021. Performance, interfacial compatibility testing and rheonaut technology analysis for simultaneous rheology and FTIR of poly (lactic acid)/modified saponite nanocomposites. Polym. Test. 100, 107232.
Chen, P., Zhou, H., Liu, W., Zhang, M., Du, Z., Wang, X., 2015. The synergistic effect of zinc oxide and phenylphosphonic acid zinc salt on the crystallization behavior of poly (lactic acid). Polym. Degrad. Stab. 122, 25–35.
Chow, T., 1980. The effect of particle shape on the mechanical properties of filled polymers. J. Mater. Sci. 15, 1873–1888.
Chu, Z., Zhao, T., Li, L., Fan, J., Qin, Y., 2017. Characterization of antimicrobial poly (lactic acid)/nano-composite films with silver and zinc oxide nanoparticles. Materials. 10 (6), 659.
Çoban, O., Bora, M.Ö., Kutluk, T., Özkoç, G., 2018. Mechanical and thermal properties of volcanic particle filled PLA/PBAT composites. Polym. Compos. 39 (S3), E1500–E1511.
Dare, M.T., Bazmi, M., Khosravi, A., Monem, M., Jafari, A., Khonakdar, H.A., 2024. Soybean oil-based nanocomposites for dye adsorption: AESO-chitosan-graphene oxide synergy in water treatment. Polym. Adv. Technol. 35 (1), e6270.
Darie-Niţă, R.N., Vasile, C., Irimia, A., Lipşa, R., Râpă, M., 2016. Evaluation of some eco-friendly plasticizers for PLA films processing. J. Appl. Polym. Sci. 133 (13).
Dayma, N., Satapathy, B.K., 2010. Morphological interpretations and micromechanical properties of polyamide-6/polypropylene-grafted-maleic anhydride/nanoclay ternary nanocomposites. Mater. Des. 31 (10), 4693–4703.
Diep, P.T.N., Takagi, H., Shimizu, N., Igarashi, N., Sasaki, S., Sakurai, S., 2019. Effects of Loading Amount of Plasticizers on Improved Crystallization of Poly (L-lactic acid). J. Fiber Sci. Technol. 75 (8), 99–111.
Díez-Pascual, A.M., Díez-Vicente, A.L., 2014. Epoxidized soybean oil/ZnO biocomposites for soft tissue applications: preparation and characterization. ACS Appl. Mater. Interfaces 6 (19), 17277–17288.
Ebadi-Dehaghani, H., Barikani, M., Khonakdar, H.A., Jafari, S.H., 2015. Microstructure and non-isothermal crystallization behavior of PP/PLA/clay hybrid nanocomposites. J. Therm. Anal. Calorim. 121, 1321–1332.
Espitia, P.J.P., Soares, N.F.F., Coimbra, J.S.R., de Andrade, N.J., Cruz, R.S., Medeiros, E. A.A., 2012. Zinc oxide nanoparticles: synthesis, antimicrobial activity and food packaging applications. Food Bioproc. Tech. 5, 1447–1464.
Farrag, Y., Barral, L., Gualillo, O., Moncada, D., Montero, B., Rico, M., Bouza, R., 2022. Effect of different plasticizers on thermal, crystalline, and permeability properties of poly (3–hydroxybutyrate–co– 3–hydroxyhexanoate) films. Polymers 14 (17), 3503.
Fornes, T., Paul, D., 2003. Modeling properties of nylon 6/clay nanocomposites using composite theories. Polymer 44 (17), 4993–5013.
Ghassemi, B., Estaji, S., Mousavi, S.R., Nemati Mahand, S., Shojaei, S., Mostafaiyan, M., Arjmand, M., Khonakdar, H.A., 2022. In-depth study of mechanical properties of poly (lactic acid)/thermoplastic polyurethane/hydroxyapatite blend nanocomposites. J. Mater. Sci. 57 (14), 7250–7264.
Giita Silverajah, V., Ibrahim, N.A., Yunus, W.M.Z.W., Hassan, H.A., Woei, C.B., 2012. A comparative study on the mechanical, thermal and morphological characterization of poly (lactic acid)/epoxidized palm oil blend. Int. J. Mol. Sci. 13 (5), 5878–5898.
Guth, E., 1945. Theory of filler reinforcement. Rubber Chem. Technol. 18 (3), 596–604.
Han, W., Liao, X., Yang, Q., Li, G., He, B., Zhu, W., Hao, Z., 2017. Crystallization and morphological transition of poly (l-lactide)–poly (ε-caprolactone) diblock copolymers with different block length ratios. RSC Adv. 7 (36), 22515–22523.
Han, Y., Shi, J., Mao, L., Wang, Z., Zhang, L., 2020. Improvement of compatibility and mechanical performances of PLA/PBAT composites with epoxidized soybean oil as compatibilizer. Ind. Eng. Chem. Res. 59 (50), 21779–21790.
Hill, R., 1964. Theory of mechanical properties of fibre-strengthened materials: I. Elastic behaviour. J. Mech. Phys. Solids 12 (4), 199–212.
Hocker, S.J., Kim, W.T., Schniepp, H.C., Kranbuehl, D.E., 2018. Polymer crystallinity and the ductile to brittle transition. Polymer 158, 72–76.
Hosseinvand, N., Eslahi, N., Abbasian, A., 2022. Properties and characterization of carrot nanocellulose/starch biopolymer nanocomposites. Polym. Compos. 43 (12), 9158–9168.
Ismail, M.F., Islam, M.A., Khorshidi, B., Tehrani-Bagha, A., Sadrzadeh, M., 2022. Surface characterization of thin-film composite membranes using contact angle technique: Review of quantification strategies and applications. Adv. Colloid Interface Sci. 299, 102524.
Jafari, A., Mirzaei, H., Shafiei, M.A., Fakhri, V., Yazdanbakhsh, A., Pirouzfar, V., Su, C. H., Ghaffarian Anbaran, S.R., Khonakdar, H.A., 2022. Conductive poly (ε-caprolactone)/polylactic acid scaffolds for tissue engineering applications: Synergy effect of zirconium nanoparticles and polypyrrole. Polym. Adv. Technol. 33 (5), 1427–1441.
Jalalifar, N., Kaffashi, B., Ahmadi, S., 2020. The synergistic reinforcing effects of halloysite nanotube particles and polyolefin elastomer-grafted-maleic anhydride compatibilizer on melt and solid viscoelastic properties of polylactic acid/polyolefin elastomer blends. Polym. Test. 91, 106757.
Jayaramudu, J., Das, K., Sonakshi, M., Reddy, G.S.M., Aderibigbe, B., Sadiku, R., Ray, S. S., 2014. Structure and properties of highly toughened biodegradable polylactide/ZnO biocomposite films. Int. J. Biol. Macromol. 64, 428–434.
Jia, P., Xia, H., Tang, K., Zhou, Y., 2018. Plasticizers derived from biomass resources: A short review. Polymers 10 (12), 1303.
Jian, X.-Y., He, Y., Li, Y.-D., Wang, M., Zeng, J.-B., 2017. Curing of epoxidized soybean oil with crystalline oligomeric poly (butylene succinate) towards high performance and sustainable epoxy resins. Chem. Eng. J. 326, 875–885.
Kaczor, D., Bajer, K., Raszkowska-Kaczor, A., Domek, G., Madajski, P., Szroeder, P., 2022. The Influence of Multiple Extrusions on the Properties of High Filled Polylactide/Multiwall Carbon Nanotube Composites. Materials. 15 (24), 8958.
Kango, S., Kalia, S., Celli, A., Njuguna, J., Habibi, Y., Kumar, R., 2013. Surface modification of inorganic nanoparticles for development of organic–inorganic nanocomposites—A review. Prog. Polym. Sci. 38 (8), 1232–1261.
Kazemi-Pasarvi, S., Ebrahimi, N.G., Raef, M., 2020. Preparation, characterization, and permeability of novel poly (lactic acid)-based blends filled with thymol and ZnO. Polym. Test. 89, 106550.
Keshavarzi, S., Babaei, A., Goudarzi, A., Shakeri, A., 2019. ZnO nanoparticles as chain elasticity reducer and structural elasticity enhancer: Correlating the degradating role and localization of ZnO with the morphological and mechanical properties of PLA/PP/ZnO nanocomposite. Polym. Adv. Technol. 30 (4), 1083–1095.
Khonakdar, H., Khasraghi, S.S., Yazdanbakhsh, A.H., Mousavi, S.R., Ahmadi, S., Arabi, H., Nobre, M.A., Khonakdar, H.A., 2024. An assessment of the role of nanosilica in thermal/thermo-oxidative degradation mechanism of poly (lactic acid)/polybutylene adipate terephthalate blend nanocomposites. Polym. Adv. Technol. 35 (4), e6374.
Khoo, R., Chow, W., 2017. Mechanical and thermal properties of poly (lactic acid)/sugarcane bagasse fiber green composites. J. Thermoplast. Compos. Mater. 30 (8), 1091–1102.
Kim, I., Viswanathan, K., Kasi, G., Sadeghi, K., Thanakkasaranee, S., Seo, J., 2019. Poly (lactic acid)/ZnO bionanocomposite films with positively charged ZnO as potential antimicrobial food packaging materials. Polymers 11 (9), 1427.
Kumar, S., Samal, S.K., Mohanty, S., Nayak, S.K., 2017. Epoxidized soybean oil-based epoxy blend cured with anhydride-based cross-linker: thermal and mechanical characterization. Ind. Eng. Chem. Res. 56 (3), 687–698.
Lee, J.H., Park, T.G., Park, H.S., Lee, D.S., Lee, Y.K., Yoon, S.C., Nam, J.-D., 2003. Thermal and mechanical characteristics of poly (L-lactic acid) nanocomposite scaffold. Biomaterials 24 (16), 2773–2778.
Li, C., Zhang, J., Han, J., Yao, B., 2021. A numerical solution to the effects of surface roughness on water–coal contact angle. Sci. Rep. 11 (1), 459.
Lim, K., Chow, W., Pung, S., 2019. Accelerated weathering and UV protection-ability of poly (lactic acid) nanocomposites containing zinc oxide treated halloysite nanotube. J. Polym. Environ. 27, 1746–1759.
Litke, Q., Wahbi, M., Kontopoulou, M., Levin, D.B., Liu, S., 2023. Epoxidized canola oil as an environmentally friendly compatibilizer for blending poly (lactic acid) and poly (butylene adipate-co-terephthalate). J. Mater. Sci. 58 (46), 17691–17710.
Lizundia, E., Penayo, M.C., Guinault, A., Vilas, J.L., Domenek, S., 2019. Impact of ZnO nanoparticle morphology on relaxation and transport properties of PLA nanocomposites. Polym. Test. 75, 175–184.
Mahmud, S., Long, Y., Abu Taher, M., Xiong, Z., Zhang, R., Zhu, J., 2019. Toughening polylactide by direct blending of cellulose nanocrystals and epoxidized soybean oil. J. Appl. Polym. Sci. 136 (46), 48221.
Mallakpour, S., Behranvand, V., 2016. Nanocomposites based on biosafe nano ZnO and different polymeric matrixes for antibacterial, optical, thermal and mechanical applications. Eur. Polym. J. 84, 377–403.
Mauck, S.C., Wang, S., Ding, W., Rohde, B.J., Fortune, C.K., Yang, G., Ahn, S.-K., Robertson, M.L., 2016. Biorenewable tough blends of polylactide and acrylated epoxidized soybean oil compatibilized by a polylactide star polymer. Macromolecules 49 (5), 1605–1615.
Meadows, S., Hosur, M., Celikbag, Y., Jeelani, S., 2018. Comparative analysis on the epoxidation of soybean oil using formic and acetic acids. Polym. Polym. Compos. 26 (4), 289–298.
Mizielińska, M., Kowalska, U., Jarosz, M., Sumińska, P., Landercy, N., Duquesne, E., 2018. The effect of UV aging on antimicrobial and mechanical properties of PLA films with incorporated zinc oxide nanoparticles. Int. J. Environ. Res. Public Health 15 (4), 794.
Mokhtari Aghdami, R., Mousavi, S.R., Estaji, S., Dermeni, R.K., Khonakdar, H.A., Shakeri, A., 2022. Evaluating the mechanical, thermal, and antibacterial properties of poly (lactic acid)/silicone rubber blends reinforced with (3-aminopropyl) triethoxysilane-functionalized titanium dioxide nanoparticles. Polym. Compos. 43 (7), 4165–4178.
Mora-Fonz, D., Lazauskas, T., Farrow, M.R., Catlow, C.R.A., Woodley, S.M., Sokol, A.A., 2017. Why are polar surfaces of ZnO stable? Chem. Mater. 29 (12), 5306–5320.
Mulla, M.Z., Rahman, M.R.T., Marcos, B., Tiwari, B., Pathania, S., 2021. Poly Lactic Acid (PLA) Nanocomposites: Effect of inorganic nanoparticles reinforcement on its performance and food packaging applications. Molecules 26 (7), 1967.
Murariu, M., Dubois, P., 2016. PLA composites: From production to properties. Adv. Drug Deliv. Rev. 107, 17–46.
Murariu, M., Doumbia, A., Bonnaud, L., Dechief, A.L., Paint, Y., Ferreira, M., Campagne, C., Devaux, E., Dubois, P., 2011. High-performance polylactide/ZnO nanocomposites designed for films and fibers with special end-use properties. Biomacromolecules 12 (5), 1762–1771.
Narkis, M., Nicolais, L., 1971. Stress–strain behavior of SAN/glass bead composites above the glass transition temperature. J. Appl. Polym. Sci. 15 (2), 469–476.
Nazir, A., Akbar, A., Baghdadi, H.B., ur Rehman, S., Al-Abbad, E., Fatima, M., Iqbal, M., Tamam, N., Alwadai, N., Abbas, M., 2021. Zinc oxide nanoparticles fabrication using Eriobotrya japonica leaves extract: Photocatalytic performance and antibacterial activity evaluation. Arab. J. Chem. 14 (8), 103251.
Nofar, M., Sacligil, D., Carreau, P.J., Kamal, M.R., Heuzey, M.-C., 2019. Poly (lactic acid) blends: Processing, properties and applications. Int. J. Biol. Macromol. 125, 307–360.
Ohama, Y., 1987. Principle of latex modification and some typical properties of latex-modified mortars and concretes adhesion; binders (materials); bond (paste to aggregate); carbonation; chlorides; curing; diffusion. Mater. J. 84 (6), 511–518.
Pantani, R., Gorrasi, G., Vigliotta, G., Murariu, M., Dubois, P., 2013. PLA-ZnO nanocomposite films: Water vapor barrier properties and specific end-use characteristics. Eur. Polym. J. 49 (11), 3471–3482.

Paul, B., 1959. Prediction of elastic constants of multiphase materials. Technical Report No. 3. Brown Univ., Providence.
Paydayesh, A., Mousavi, S.R., Estaji, S., Khonakdar, H.A., Nozarinya, M.A., 2022. Functionalized graphene nanoplatelets/poly (lactic acid)/chitosan nanocomposites: Mechanical, biodegradability, and electrical conductivity properties. Polym. Compos. 43 (1), 411–421.
PP, V., 2020. In vitro biocompatibility and antimicrobial activities of zinc oxide nanoparticles (ZnO NPs) prepared by chemical and green synthetic route—a comparative study. BioNanoScience 10 (1), 112–121.
Quiles-Carrillo, L., Duart, S., Montanes, N., Torres-Giner, S., Balart, R., 2018. Enhancement of the mechanical and thermal properties of injection-molded polylactide parts by the addition of acrylated epoxidized soybean oil. Mater. Des. 140, 54–63.
Raghunath, S., Kumar, S., Samal, S.K., Mohanty, S., Nayak, S.K., 2018. PLA/ESO/MWCNT nanocomposite: a study on mechanical, thermal and electroactive shape memory properties. J. Polym. Res. 25, 1–12.
Rao, P.JM., 2007. Mechanics of polymer− clay nanocomposites. Macromolecules 40 (2), 290–296.
Restrepo, I., Flores, P., Rodríguez-Llamazares, S., 2019. Antibacterial nanocomposite of poly (lactic acid) and ZnO nanoparticles stabilized with poly (vinyl alcohol): thermal and morphological characterization. Polym.-Plast. Technol. Mater. 58 (1), 105–112.
Rokbani, H., Ajji, A., 2018. Rheological properties of poly (lactic acid) solutions added with metal oxide nanoparticles for electrospinning. J. Polym. Environ. 26, 2555–2565.
Shankar, S., Rhim, J.-W., 2019. Effect of types of zinc oxide nanoparticles on structural, mechanical and antibacterial properties of poly (lactide)/poly (butylene adipate-co-terephthalate) composite films. Food Packag. Shelf Life 21, 100327.
Shankar, S., Wang, L.-F., Rhim, J.-W., 2018. Incorporation of zinc oxide nanoparticles improved the mechanical, water vapor barrier, UV-light barrier, and antibacterial properties of PLA-based nanocomposite films. Mater. Sci. Eng. C 93, 289–298.
Shojaeiarani, J., Bajwa, D., Jiang, L., Liaw, J., Hartman, K., 2019. Insight on the influence of nano zinc oxide on the thermal, dynamic mechanical, and flow characteristics of Poly (lactic acid)–zinc oxide composites. Polym. Eng. Sci. 59 (6), 1242–1249.
Silverajah, V.G., Ibrahim, N.A., Zainuddin, N., Yunus, W.M.Z.W., Hassan, H.A., 2012. Mechanical, thermal and morphological properties of poly (lactic acid)/epoxidized palm olein blend. Molecules 17 (10), 11729–11747.
Taguet, A., Cassagnau, P., Lopez-Cuesta, J.-M., 2014. Structuration, selective dispersion and compatibilizing effect of (nano) fillers in polymer blends. Prog. Polym. Sci. 39 (8), 1526–1563.
Tajdari, A., Babaei, A., Goudarzi, A., Partovi, R., 2020. Preparation and study on the optical, mechanical, and antibacterial properties of polylactic acid/ZnO/TiO2 shared nanocomposites. J. Plast. Film Sheeting 36 (3), 285–311.
Tan, M.A., Yeoh, C.K., Teh, P.L., Rahim, N.A.A., Song, C.C., Voon, C.H., 2023. Effect of zinc oxide suspension on the overall filler content of the PLA/ZnO composites and cPLA/ZnO composites. e-Polymers 23 (1), 20228113.
Tang, Z., Fan, F., Chu, Z., Fan, C., Qin, Y., 2020. Barrier properties and characterizations of poly (lactic acid)/ZnO nanocomposites. Molecules 25 (6), 1310.
Tayebi, P., Asefnejad, A., Khonakdar, H.A., 2021. Water-based polyurethane/functionalized chitosan/zinc oxide nanoparticles nanocomposites: physical, mechanical and biocompatibility properties. Polym.-Plast. Technol. Mater. 60 (13), 1474–1489.
Tayouri, M.I., Mousavi, S.R., Estaji, S., Nemati Mahand, S., Jahanmardi, R., Arjmand, M., Arnhold, K., Khonakdar, H.A., 2022. Polystyrene/polyolefin elastomer/halloysite nanotubes blend nanocomposites: Morphology-thermal degradation kinetics relationship. Polym. Adv. Technol. 33 (7), 2149–2165.
Tayouri, M.I., Estaji, S., Mousavi, S.R., Yazdanbakhsh, A., Nouranian, S., Ruckdäschel, H., Khonakdar, H.A., 2023. Polystyrene/Polyolefin Elastomer Blends Loaded with Halloysite Nanotubes: Morphological, Mechanical, and Gas Barrier Properties. Macromol. Mater. Eng. 2300080.
Thakur, S., Chaudhary, J., Singh, P., Alsanie, W.F., Grammatikos, S.A., Thakur, V.K., 2022. Synthesis of Bio-based monomers and polymers using microbes for a sustainable bioeconomy. Bioresour. Technol. 344, 126156.
Thanakkasaranee, S., Kim, D., Seo, J., 2018. Preparation and characterization of poly (ether-block-amide)/polyethylene glycol composite films with temperature-dependent permeation. Polymers 10 (2), 225.
Wang, S., Liu, B., Qin, Y., Guo, H., 2021. Effects of processing conditions and plasticizing-reinforcing modification on the crystallization and physical properties of PLA films. Membranes 11 (8), 640.
Wu, T.-M., Wu, C.-Y., 2006. Biodegradable poly (lactic acid)/chitosan-modified montmorillonite nanocomposites: Preparation and characterization. Polym. Degrad. Stab. 91 (9), 2198–2204.
Xie, J., Gu, K., Zhao, Y., Yao, J., Chen, X., Shao, Z., 2022. Enhancement of the Mechanical Properties of Poly (lactic acid)/Epoxidized Soybean Oil Blends by the Addition of 3-Aminophenylboronic Acid. ACS Omega 7 (21), 17841–17848.
Xiong, Z., Yang, Y., Feng, J., Zhang, X., Zhang, C., Tang, Z., Zhu, J., 2013. Preparation and characterization of poly (lactic acid)/starch composites toughened with epoxidized soybean oil. Carbohydr. Polym. 92 (1), 810–816.
Xu, Y.Q., Qu, J.P., 2009. Mechanical and rheological properties of epoxidized soybean oil plasticized poly (lactic acid). J. Appl. Polym. Sci. 112 (6), 3185–3191.
Yan, Y.-F., Liang, X.-B., Feng, Y.-L., Shi, L.-F., Chen, R.-P., Guo, J.-Z., Guan, Y., 2023. Manipulation of crystallization nucleation and thermal degradation of PLA films by multi-morphologies CNC-ZnO nanoparticles. Carbohydr. Polym. 320, 121251.
Yang, J., Wang, J., Li, X., Lang, J., Liu, F., Yang, L., Zhai, H., Gao, M., Zhao, X., 2012. Effect of polar and non-polar surfaces of ZnO nanostructures on photocatalytic properties. J. Alloy. Compd. 528, 28–33.
Yu, F., Fei, X., He, Y., Li, H., 2021. Poly (lactic acid)-based composite film reinforced with acetylated cellulose nanocrystals and ZnO nanoparticles for active food packaging. Int. J. Biol. Macromol. 186, 770–779.
Zamanian, M., Ashenai Ghasemi, F., Mortezaei, M., 2021. Interphase characterization and modeling of tensile modulus in epoxy/silica nanocomposites. J. Appl. Polym. Sci. 138 (5), 49755.
Żenkiewicz, M., Richert, J., Rytlewski, P., Moraczewski, K., 2009. Some effects of corona plasma treatment of polylactide/montmorillonite nanocomposite films. Plasma Processes Polym. 6 (S1), S387–S391.
Zhang, H., Hortal, M., Jordá-Beneyto, M., Rosa, E., Lara-Lledo, M., Lorente, I., 2017. ZnO-PLA nanocomposite coated paper for antimicrobial packaging application. Lwt. 78, 250–257.
Zhao, L., Jia, S.-L., Wang, Z.-P., Chen, Y.-J., Bian, J.-J., Han, L.-J., Zhang, H.-L., Dong, L.-S., 2021. Thermal, rheological and mechanical properties of biodegradable poly (propylene carbonate)/epoxidized soybean oil blends. Chin. J. Polym. Sci. 39, 1572–1580.
Zhao, Y., Qu, J., Feng, Y., Wu, Z., Chen, F., Tang, H., 2012. Mechanical and thermal properties of epoxidized soybean oil plasticized polybutylene succinate blends. Polym. Adv. Technol. 23 (3), 632–638.
Zhuang, Y.X., Hansen, O., 2009. Correlation of effective dispersive and polar surface energies in heterogeneous self-assembled monolayer coatings. Langmuir 25 (10), 5437–5441.